24th COBEM - 2017

24th ABCM International Congress of Mechanical Engineering
December 3-8, 2017, Curitiba, PR, Brazil

COBEM-2017-0989
THREE-DIMENSIONAL VISUALIZATION OF OIL DISPLACEMENT BY FLEXIBLE MICROCAPSULES SUSPENSIONS IN POROUS MEDIA

José Ronaldo Vimieiro Júnior
Débora Freitas do Nascimento
Márcio da Silveira Carvalho

Pontifícia Universidade Católica do Rio de Janeiro, Rua Marquês de São Vicente, 225, Gávea, Rio de Janeiro/RJ - Brasil
msc@puc-rio.br

Abstract. *In a globalized world, the demand for energy is always growing. Since the oil and gas industry is responsible for delivering most of this demand, this makes hydrocarbon components increasingly important in the worldwide economy. However, such resources are finite, so a conscious exploration always seeking the maximum performance is required. As oil reservoirs after the application of primary and secondary recovery techniques usually still have about 65% of the original oil volume contained in their pores, methods that aim its reduction are gaining an increasingly important role in the energy industry. In this context, this work presents a three-dimensional micromodel representative of a porous medium that is used for pore-scale flow analysis. Confocal microscopy is used to visualize the microscale phenomena, leading to specific information about ganglia dynamics, related to its formation, mobilization and entrapment. The residual oil saturation, an important value to measure the amount of oil produced in a given reservoir is determined for different flow conditions. The results show that the suspensions composed by flexible microcapsules could be used as a mobility control agent, since it modifies the fluid distribution in the porous media, which results on the improvement of the pore scale displacement efficiency, and consequently reducing the residual oil saturation.*

Keywords: *Enhanced Oil Recovery, Suspensions, Confocal Microscopy, Microfluidics*

1. INTRODUCTION

The recent global increase in energy demand has made hydrocarbon components increasingly important on the world market, as this current energy demand is expected to be supplied by the oil and gas industry (BP, 2016). However, it is known that this is a finite natural resource and the worldwide reserves of these materials are in decline, which promotes the need of a conscious and efficient exploration of such resources.

The application of enhanced oil recovery (EOR) methods is a manner used to increase the efficiency of reservoirs. After the primary recovery, reservoirs could still have about 65% of oil remaining in their pores (Thomas, 2008). Recently, different EOR methods such as chemical, miscible, thermal and biological, emerged as a research target with the aim of improve the macroscopic sweep and reduce the residual oil saturation in the reservoir. Experimental works covering the macroscopic scale, like core flooding, have been explored in the literature to assess the efficiency of the different methods. However, the macroscopic scale experiments do not enable the analysis of phenomena that occur in the pore scale. Experimental work in microscopic scale has also been performed, aiming to reduce this gap left by macroscopic experiments, such as the work of Nilsson *et al.* (2013) who have developed a microfluidic device to test the performance of different fluids with distinct rheological properties applied in enhanced oil recovery.

The analysis of the physical phenomena that happen in the pore scale is usually obtained through visualization techniques of two-dimensional micromodels (Lenormand, 1986; Galindo-Rosales *et al*., 2012; Bento and Moreno, 2016). These devices consists in a transparent artificial structures developed to represent the complexity of the porous media and to promote the process investigation of oil displacement by different fluids. Even though the two-dimensional analysis has been extensively used, they do not provide an accurate representation of the porous space, since such structure is in fact three-dimensional. Therefore, there is a need to investigate these phenomena in a realistic and effective way, through three-dimensional visualization and analysis. Despite its great practical importance, a clear idea about the determination of the flow through 3D micromodels remains unclear in the literature due to its high complexity.

Therefore, in order to analyze the physical phenomena that occur in the pore scale an experimental procedure in three-dimensional porous media will be described in this work, using special visualization techniques. These studies will elucidate the understanding of the dynamics of formation, mobilization and entrapment of oil ganglia, as well as the analysis of the residual oil saturation under a multiphase flow. The oil displacement process will be made first by water injection to evaluate the influence of capillary number in the residual oil saturation (SOR) and then by microcapsules suspension injection, which is an EOR method used to reduce the volume of oil entrapped.

2. EXPERIMENTAL METHODOLOGY

The oil displacement experiments were performed on a 3D porous media, as shown in Fig. 1, prepared by lightly sintering densely packed hydrophilic glass beads, with radii a = 214.61 ± 5.1 μm, in thin walled rectangular quartz capillaries of cross sectional area A = 9 mm². The packings have length L = 3 cm (Krummel *et al* 2013; Datta *et al.* 2014).

Figure 1. 3D Micromodel (Quartz capillary with packed glass beads)

Scattering of light from the surfaces of the beads typically precludes direct observation of the multiphase flow within the 3D medium. This limitation is overcome by formulating Newtonian fluids designed to match the refractive index of the glass beads, enabling the visualization of the multiphase flow in 3D (Walmann, 1992; Frette *et al.*, 1994; Stöhr *et al.*, 2003; Sharma, 2011). The non-wetting fluid is a mixture of oils (82.03 wt% immersion oil, 6350 of Cargille & 17.97 wt% lubricant oil, Schulz of Waynoil), which is denominated oil phase. Its dynamic viscosity (μ_{nw}) is 106.84 mPa.s at 24°C. The wetting fluid (aqueous phase) is a mixture of 54.006 wt% of dimethyl sulfoxide, 31.87 wt% of sucrose, 13.72 wt% of Milli-Q® water from Millipore Corporation and 0.394 wt% of Fluorescein. The dynamic viscosity (μ_w) of the wetting fluid is 33.68 MPa.s at 24°C. Both viscosities were measured using a stress-controlled rheometer. The viscosity ratio between the phases is $M = \mu_w / \mu_{nw} \sim 0.315$. The densities of the wetting fluid and the non-wetting fluid are $\rho_w = 1.2202$ g/mL and $\rho_o = 0.8699$ g/mL, respectively. The two fluids are fully immiscible over the experimental timescale. The interfacial tension between the phases is $\sigma = 22.2$ mN/m, measured using a du Noüy ring.

Prior to the experiments, the micromodel was characterized in relation to its porosity and permeability. The porosity is found by diving the device into the water. The pore space is filled with water. The pore volume is evaluated by the difference between the weight of dry micromodel and wet micromodel. The pore volume divided by the total volume represents the effective porosity of the device. The effective porosity was found to be 43.19 ± 0.8 %. A differential pressure sensor is used to measure the pressure drop ΔP across the porous medium with legth L and cross sectional area A, during the variation of the flow rate Q, this enables the determination of the absolute permeability using the Darcy's law, $k/\mu = (Q/A)/(\Delta P/L)$, once the fluid viscosity is known. The absolute permeability was found to be 14.21 ± 1.0 D.

Preceding each experiment, the micromodel is saturated with CO_2 gas, this gas is soluble in the wetting fluid, preventing the formation of any trapped gas bubbles which may influence the results. The experimental apparatus, shown in Fig. 2, consists of a syringe pump (Harvard Apparatus) used for injecting the different fluids (oil phase and aqueous phase). All experiments are performed using gastight glass syringes (Hamilton). The termination in Teflon with Luer-Lock coupling provides easy connection with the 1/32" internal diameter plastic tubing. A DMi8 microscope from Leica Microsystems Inc., equipped with confocal TCS SP8 is used to image the 3D stacks of the micromodel.

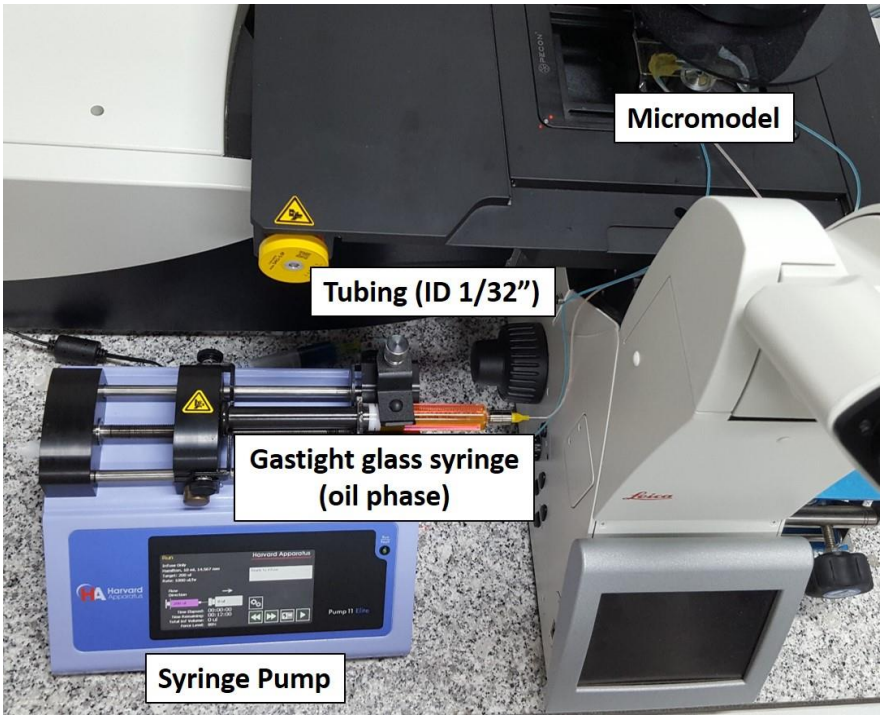

Figure 2. Experimental Setup

To visualize the pore structure in 3D, 168 optical slices were acquired, each one spaced by 2.41 μm along z-direction within the porous medium. The images have 512x512 pixels with resolution of 1.137x1.137x2.407 μm³ in the directions x/y/z, respectively. These optical slices were used to reconstruct the 3D structure. In all experiments, the porous media is initially saturated with the wetting fluid in order to map the pore structure, once the glass beads and the oil phase do not have fluorophores, thus, they are not detected by the confocal microscope. Then the micromodel is saturated with the oil phase with a constant flow rate Q = 1mL/h, process known as primary drainage, this step concludes the micromodel preparation.

Once the 3D images are acquired, they are processed to extract numerical attributes and then perform quantitative analysis. The general idea is transform an image into a binary image, enabling the computer interpretation. Usually the image processing is divided in three blocks: Acquisition, Processing and Analysis (Vieira, 2001). However image processing of three-dimensional images is more complex than two-dimensional ones. Robust mathematical algorithms must be used to support the computer decision about the thresholding limit selection. A flowchart, shown in Fig. 3, was developed and applied in the images acquired in this work.

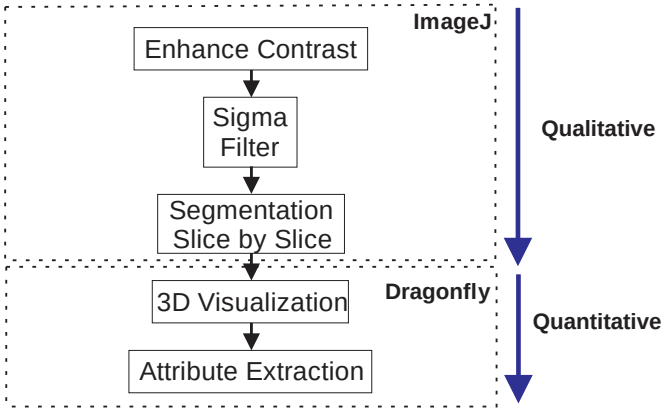

Figure 3. Flowchart of 3D image processing

The image processing begins enhancing the image contrast to balance the fluorescence intensity variation on z direction which happens due to light scattering. By doing this, the noise associated to the image is also increased, and then the filter is used to reduce such noise. Then we start the segmentation, which is the most important step in the

image processing. This step was made slice by slice using the mathematical method of Lee (Li, 1993; Li, 1998). The image processing was performed using ImageJ and Dragonfly softwares.

The experimental procedure is divided into two parts. The first analyses the effect of capillary number, defined in Equation 1, on the oil ganglia distribution by varying the water injection flow rate. The second part consists in the assessment of the microcapsules suspension as an agent for mobility control of the displacing fluid, in other words, the analysis of the method as an EOR technique.

$$Ca = \frac{\mu v}{\sigma} \tag{1}$$

3. RESULTS

3.1 Water Injection

These experiments were performed at controlled flow rates to investigate the effect of capillary number in the residual oil saturation and ganglia distribution. To visualize the dynamics of fluid displacement, a series of optical slices were acquired at a fixed z position using the confocal microscope, several bead diameters deep within the medium, at multiple xy locations spanning a significative length of the medium. The analysis is restricting to an area away from each edge of the medium to minimize boundary effects.

The displacement of the non-wetting fluid by the wetting fluid leads to the formation of discrete oil ganglia, many of them remained trapped within the pore space. In order to explore the variation of the residual oil saturation with the imposed flow conditions, Ca varied from 10^{-6} to $6.25x10^{-4}$. For each value of Ca the wetting fluid was injected into the micromodel at a fixed flow rate until oil production ceases establishing a steady state.

Fig. 4 illustrates the results of the tests performed with porous media A and D at Ca = $1x10^{-6}$, $5x10^{-6}$, $2.5x10^{-5}$, $1.25x10^{-4}$ and $6.25x10^{-4}$, respectively. The images 4.I and 4.II represent the micromodel preparation previously described. The images 4.III, 4.IV, 4.V, 4.VI and 4.VII show the experiments' steps, thus, the injection of aqueous phase until oil is no longer produced.

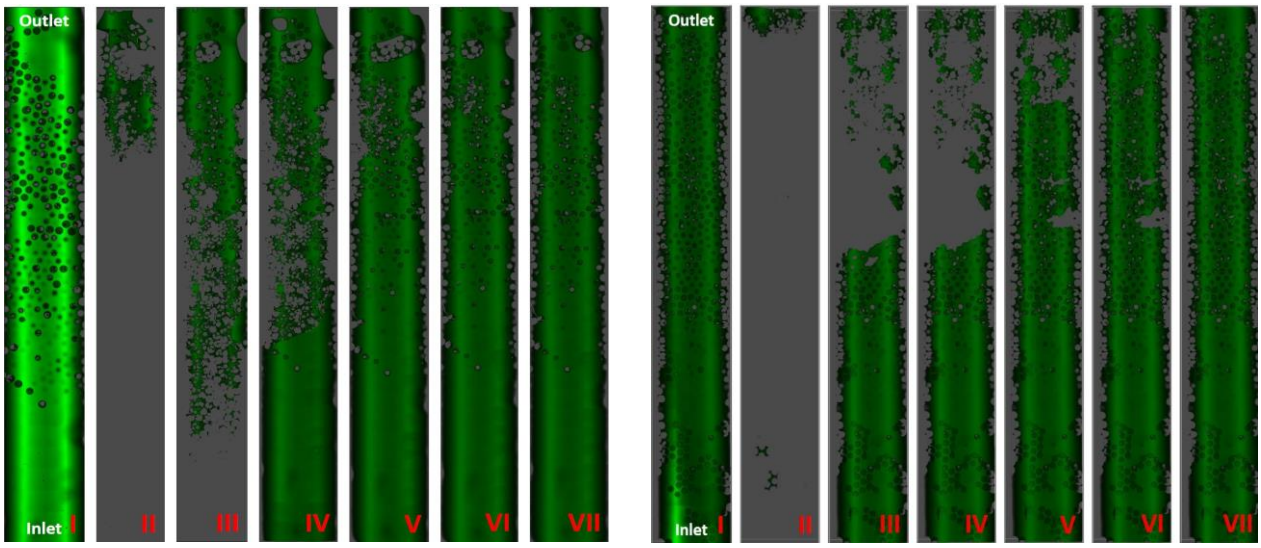

Figure 4. Different test's phases on porous media A and D

The same procedure was applied for different micromodels. The plot shown in Fig. 5 presents the capillary desaturation curves for all water injection tests. This curve relates the residual oil saturation with the capillary number and is the experimental observation most commonly used in oil recovery as it reveals flow conditions required for acceptable oil displacement in porous media (Yeganeh, 2016).

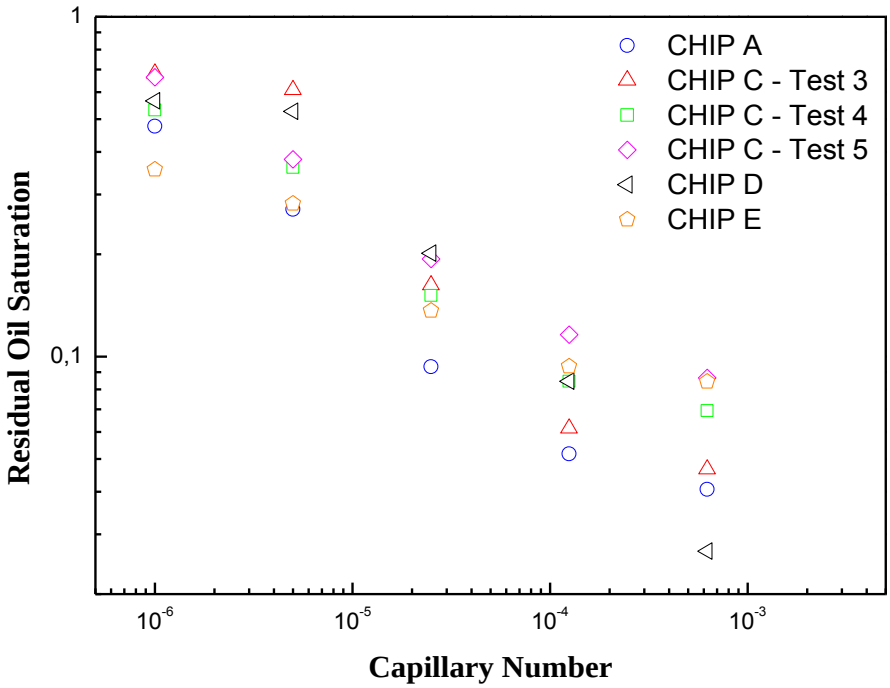

Figure 5. Capillary desaturation curves

The results presented so far match the results found in the literature. It is clear in the curves of Fig. 5 that increasing the capillary number leads to lower residual oil saturation. It is also possible to note that the different micromodels have the same behavior, once the glass beads packing process is the same, thus, they have approximately the same properties (porosity and permeability).

The ganglia size distribution after each step of the experiment is analyzed through image processing. A three-dimensional image enables the qualitative analysis of the ganglia volume, as shown in the Fig. 6, which presents the first and last step of the experiment in test 3 of micromodel C.

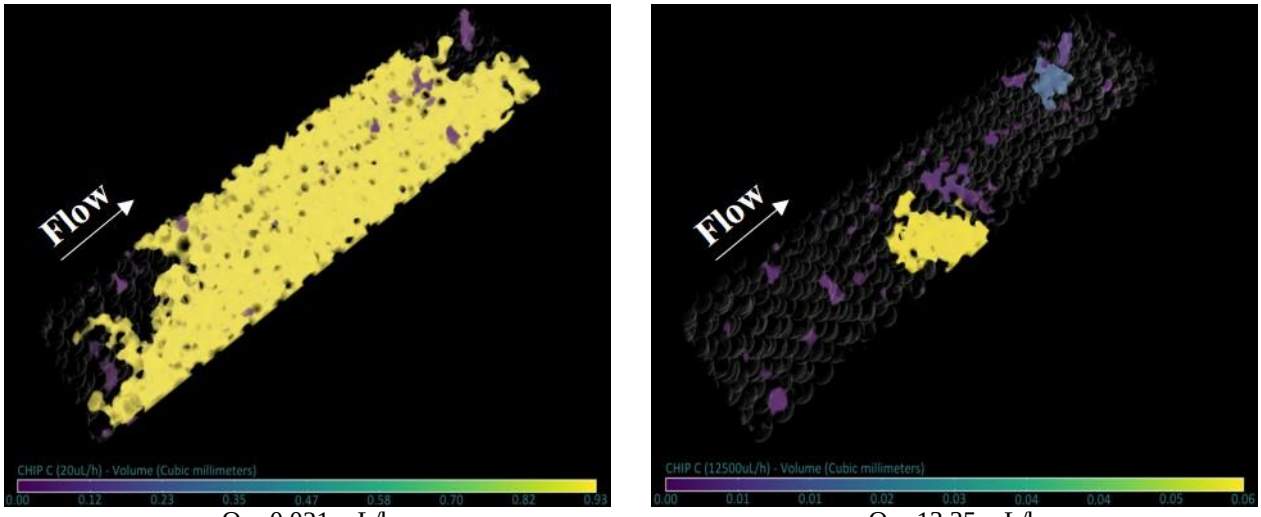

Q = 0.021 mL/h Q = 13.35 mL/h

Figure 6. Reduction of residual oil saturation

The quantitative analysis shows that as the capillary number increases, the number of oil ganglia increases as well. Nevertheless, these oil ganglia are very small, which leads to a lower residual oil saturation. To elucidate this statement a quantitative analysis was performed using the numerical attributes extracted from the images previously introduced. Two histograms using the data of all tests of water injection were designed (Fig. 7). The first one shows the oil ganglia frequency for a given volumetric class and the second one presents the oil volume for the same volumetric class as complementary information.

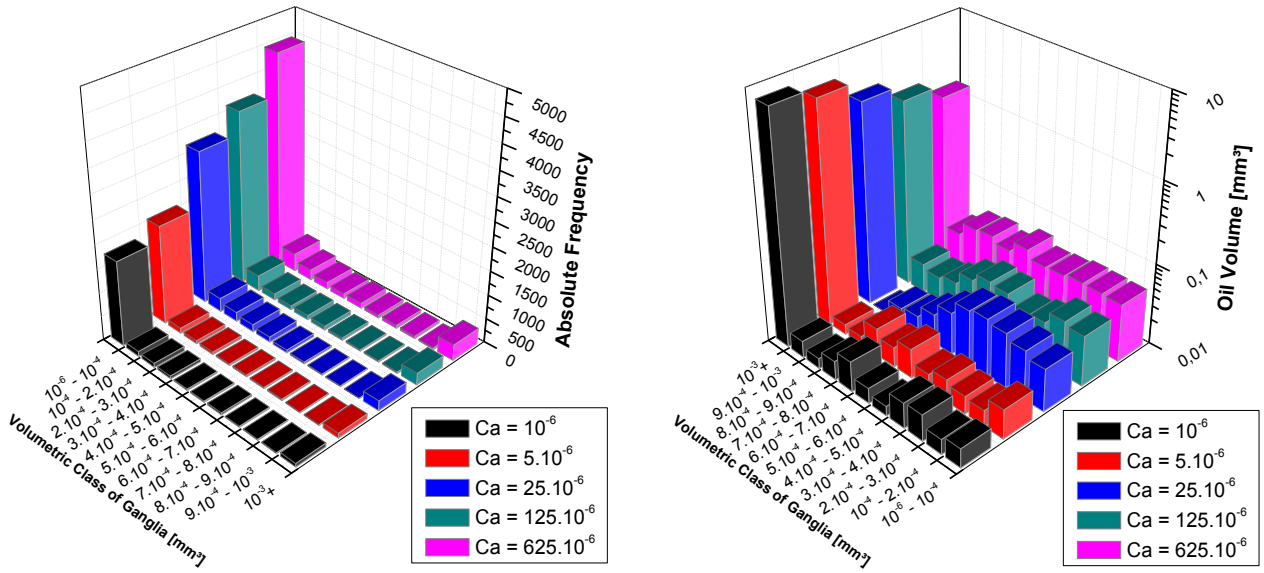

Figure 7. Histograms of oil ganglia frequency and oil ganglia volume

3.2 Microcapsules Suspension Injection

With the validation of the experimental procedure and the image processing flowchart through the previously performed tests, the microcapsules suspensions are prepared to be injected into the micromodels. The microcapsules suspension were characterized in terms of their size and mechanical properties. Since the porous structure is composed by glass beads with mean diameter of 214.61µm, it is possible to calculate the approximate pore throat size. The literature presents several different ways to perform this calculation, the experimental work of Dias *et al*. (2007) estimates the pore throat diameter as a function of particle diameter and porosity:

$$Dpore = \frac{2Dparticle}{3} \times \frac{\phi}{(1-\phi)} \tag{2}$$

Therefore, since the pore diameter is related to the porosity of the medium and each microdevice has a different effective porosity, the value used in this variable is the arithmetic mean of the effective porosity of all devices used in this work. Thus, the pore mean diameter calculated with Eq. (2) is D_{pore} = 110.06µm. The microcapsules suspensions goal is to block the preferential pathways previously performed by the displacing fluid, consequently, such particles must have mean diameter larger than 110.06µm. With this value as reference microcapsules with mean diameter ranging from 150 to 250µm were produced. This range has been chosen so that the microcapsules do not easily flow through the pores, being blocked in some of these pores, diverting the displacing fluid flow, and passing through others pores because they are flexible.

The experiments of microcapsule suspension injection were performed using different properties of these particles in order to assess the role of capsule mechanical properties. In the first test the ratio of polymer to crosslinker was 10:1, these particles have a mean diameter of 218.3µm with a standard deviation of 4.1, and mean shell thickness of 16.6µm with standard deviation of 1.7 (Fig.8).

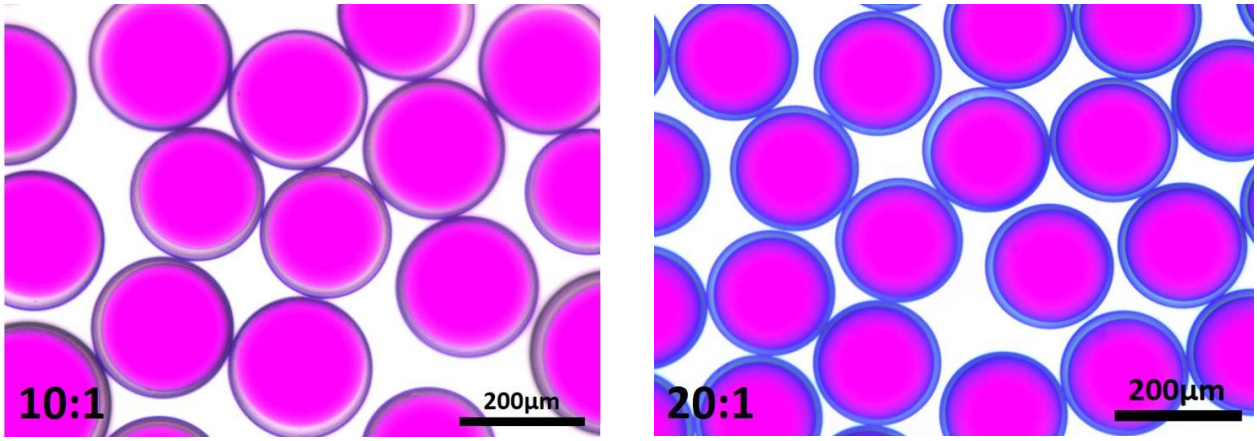

Figure 8. Microcapsules suspensions

The test consists in two steps: The first step consists of water injection in a fixed flow rate until the production of oil ceased, reaching the steady state. The second step represents the microcapsules suspension injection in the same flow rate of the previous phase, also until the steady state was reached. Three tests were performed using microdevices C, D and E. The flow rate (Q) used was 0.107 mL/h. Fig. 9 shows the images of the four steps of one single test performed with microdevice D, where the images 9.I and 9.II represent the micromodel preparation and images 9.III and 9.IV represent the injection of the aqueous phase and microcapsules suspension, respectively.

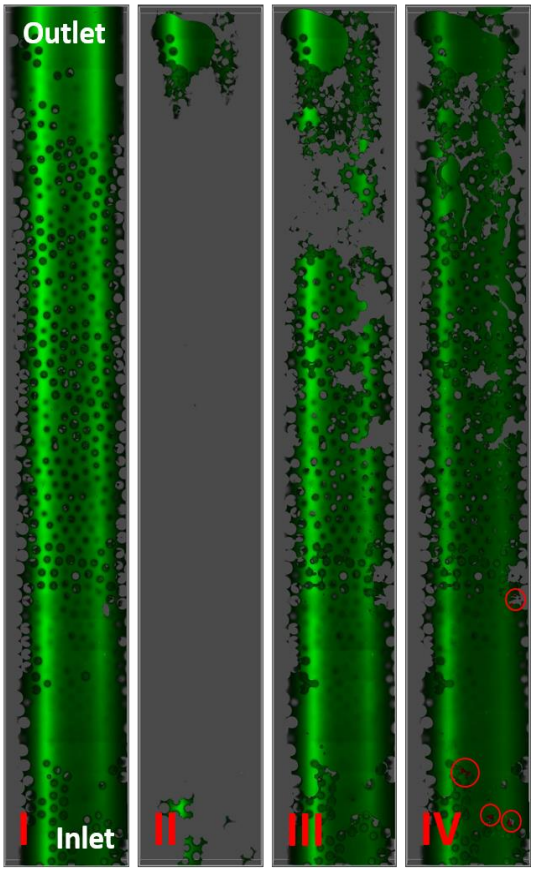

Figure 9. Test's steps of microcapsules suspension injection in microdevice D

The red circles in the Fig. 9.IV indicate the location where the microcapsules were trapped. They are blocking the pathways of the displacing fluid and forcing it to go through another pathway, displacing the oil ganglia trapped along this new route, thereby reducing the residual oil saturation. The concentration of microcapsules was kept the same for all tests performed enabling the comparison between them. Fig. 10 presents the final saturation of the tests in microdevices C, D and E showing the microcapsules distribution in the micromodel after the steady state.

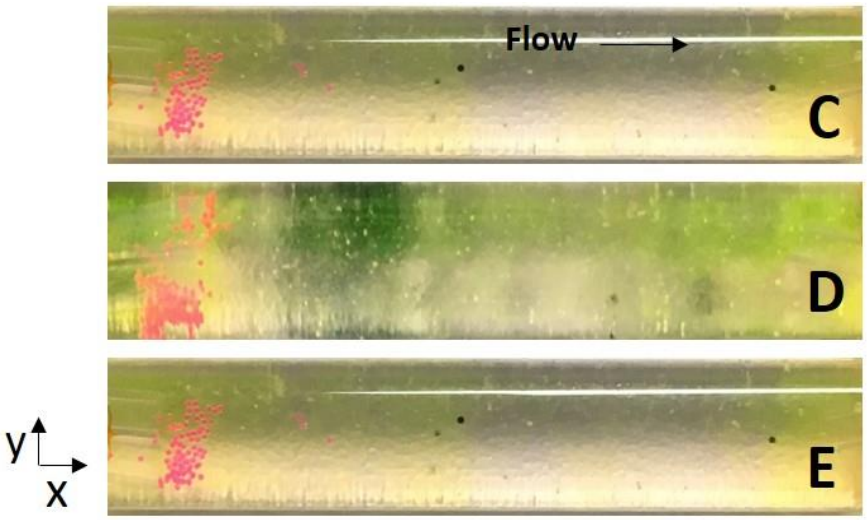

Figure 10. Distribution of the microcapsules

It is possible to note that the flexibility of the 10:1 microcapsules was not enough to make them penetrate deeper into the micromodel. That is the reason of the production of 20:1 microcapsules showed in Fig. 8. These particles have a mean diameter of 197µm with a standard deviation of 5.2, and mean shell thicknesses of 12.4µm with standard deviation of 1.3. A test was performed using microdevice F, following the same procedure of preparation and the same flow rate of the previous tests. Also, in this new test the flow rate was increased to 2.67 mL/h. With this last test, it is evidenced that the 20:1 microcapsules are also not flexible enough to penetrate into the porous medium, even with a significant increase of the flow rate. Therefore, both types of microcapsules were not able to penetrate deeper into the mmicrodevices due to its relation of flexibility and particle size with the pore throat size. Because the capsules were trapped near the inlet, the reduction on residual oil saturation is not very significant, as shown in Fig. 11.

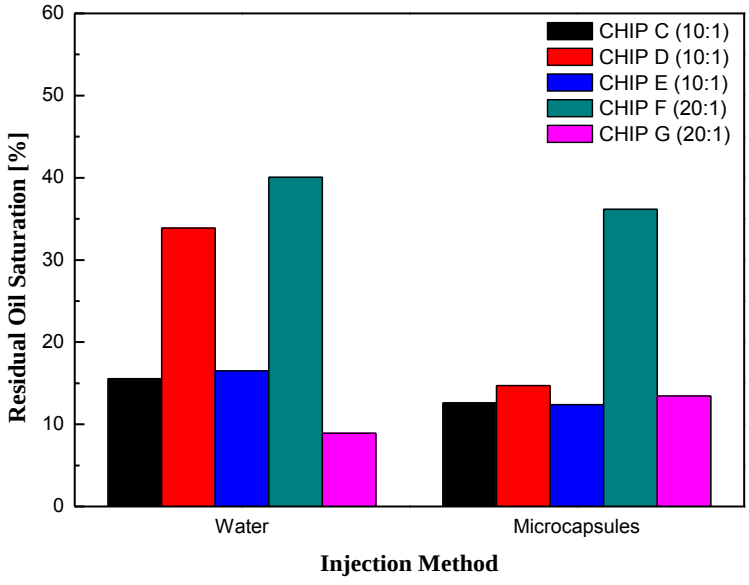

Figure 11. Decrease of residual oil saturation with microcapsules injection

Fig. 11 shows that for the microdevice G, after the injection of microcapsules suspension the residual oil saturation did not decrease. This can be explained due to the fact that the micromodel has 3000 µm of depth, and the technology used to map this porous medium, with all the adjustments made, has reached 400 µm in depth. Therefore, oil that was in the section not mapped by the microscope was displaced by the high flow rate imposed to the mapped section, increasing the residual oil saturation in the last step of the test. It is important to mention that the technology applied in this work to scan the micromodel are in the state-of-the-art, thus, 400 µm in depth is the highest value possible to reach.

4. FINAL REMARKS

This work deals with the analysis of the oil displacement through the injection of water and suspensions of flexible microcapsules, in which the main objective is to investigate the flow dynamics in three-dimensions, since the literature mostly presents two-dimensional analysis of these phenomena. It also aims to quantify the residual oil saturation for different flow conditions, and evaluate the method as an enhanced oil recovery technique, acting as a mobility control agent.

In this context, an experimental procedure arrangement was developed for the problem under consideration. First, a review of the theoretical aspects related to the physics was introduced. Afterwards, an experimental methodology was presented to elucidate the step-by-step of the experiments, which consisted in describing the preparation and characterization of the micromodel used to represent the porous medium, development of the aqueous and oil phases as immiscible fluids. Finally, a methodology of digital image processing was demonstrated, since the images acquired with the confocal microscope do not provide numerical attributes.

The results were demonstrated that by increasing the capillary number, the residual oil saturation decreases and the number of ganglia increases. These results were validated according to some experimental studies available in the literature, such those presented by Payatakes (1982), Melrose & Brandner (1974) and Guillen *et al*. (2012).

The second section of results presented the tests in which microcapsules suspensions were injected, in order to evaluate the use of such technique in the mobility control of the displacing fluid. It was observed that for microcapsules of ratio 10:1 in the polymer and cross linker, the flexibility of these particles was not enough for them to penetrate the entire body of the porous medium, thus being trapped early in the micromodel. Microcapsules of ratio 20:1 were thus produced, but it was equally observed that these microcapsules also do not have sufficient flexibility to penetrate deeper the micromodel, even with the drastic increase of the flow rate. However, it was possible to observe an important role of these microcapsules suspensions as an EOR technique, for both cases the residual oil saturation decreased.

5. ACKNOWLEDGEMENTS

This work was carried out in association with the ongoing Project registered as “Escoamento de dispersões complexas em meios porosos heterogêneos: análise na escala de poro e macrocópica” (PUC-Rio/Shell Brasil/ANP) – Complex Dispersion Flow Through Porous Media – funded by Shell Brasil under the ANP R&D levy as “Compromisso de Investimentos com Pesquisa e Desenvolvimento”.

6. REFERENCES

Bento, H. L. I. and Moreno, R. B. Z. L., 2016. “Evaluation of heavy oil recovery factor by water flooding and polymer flooding at different temperatures”. *SPE Latin America and Caribbean Heavy and Extra Heavy Oil Conference*. 19-20 October, Lima, Peru. DOI: 10.2118/181193-MS.

BP, 2016. *Annual Report* 2015.

Datta, S. S., Ramakrishnan, T. S. and Weitz, D. A., 2014. “Mobilization of a trapped non-wetting fluid from a three-dimensional porous medium”. *Physics of Fluids*, Vol. 26, n. 2, p. 022002. DOI: 10.1063/1.4866641.

Dias, R. P. *et al*., 2007. “Permeability and effective thermal conductivity of bisized porous media”. *International Jounal of Heat and Mass Transfer*, Vol. 50, n. 7-8, p. 1295-1301. DOI: 10.1016/j.ijheatmasstransfer.2006.09.039.

Frette, V. *et al*., 1994. “Fast, immiscible fluid-fluid displacement in three-dimensional porous media at finite viscosity constrast”. *Physical Review E*, Vol. 50, n.4. DOI: 10.1103/PhysRevE.50.2881.

Galindo-Rosales, F. J. *et al*., 2012. “Microfluidic systems for analysis of viscoelastic fluid flow phenomena in porous media”. *Microfluidics and Nanofluidics*, Vol. 12, n. 1-4, p. 485-498. DOI: 10.1007/s10404-011-0890-6.

Guillen, V. R., Carvalho, M. S. and Alvarado, V., 2012. “Pore scale and macroscopic displacement mechanisms in emulsion flooding”. *Transport in Porous Media*, Vol. 94, n. 1, p. 197-206. DOI: 10.1007/s11242-012-9997-9.

Krummel, A. T. *et al.*, 2013. “Visualizing multiphase flow and trapped fluid configurations in a model three-dimensional porous medium”. *AIChE Journal*, Vol. 59, n. 3, p. 1022-1029. DOI: 10.1002/aic.14005.

Lenormand, R., 1986. “Pattern growth and fluid displacements through porous media”. *Physica A: Statistical Mechanics and its Application*, Vol. 140, n. 1-2, p. 114-123. DOI: 10.1016/0378-4371(86)90211-6.

Li, C. H. and Lee, C. K., 1993. “Minimum cross entropy thresholding”. *Pattern Recognition*, Vol. 26, n. 4, p. 617-625. DOI: 10.1016/0031-3203(93)90115-D.

Li, C. H. and Tam, P. K. S., 1998. “An interative algorithm for minimum cross entropy thresholding”. *Pattern Recognition Letters*, Vol. 19, n. 8, p. 771-776. DOI: 10.1016/SO167-8655(98)00057-9.

Melrose, J. C. and Brandner, C. F., 1974. “Role of capillary forces in determining microscopic displacement efficiency for oil recovery by waterflooding”. *Journal of Canadian Petroleum Technology*, Vol. 13, n. 4. DOI:10.2118/74-04-05.

Nilsson, M. A. *et al*., 2013. “Effect of fluid rheology on enhanced oil recovery in a microfluidic sandstone device”. *Journal of Non-Newtonian Fluid Mechanics*, Vol. 202, p. 112-119. DOI: 10.1016/j.jnnfm.2013.09.011.

Payatakes, A. C., 1982. "Dynamics of oil ganglia during immiscible displacement in water-wet porous media". *Annual Review of Fluid Mechanics*, Vol. 14, n. 1, p. 365-393. DOI: 10.1146/annurev.fl.14.010182.002053.

Sharma, P. *et al*., 2011. "Three-dimensional real-time imaging of bi-phasic flow through porous media". *Review of Scientific Instruments*, Vol. 82, p. 113704. DOI: 10.1063/1.3658822.

Stöhr, M., Roth, K. and Jähne, B., 2003. "Measurement of 3D pore scale flow in index-matched porous media". *Experiments in Fluids*, Vol. 35, n. 2, p. 159-166. DOI: 10.1007/s00348-003-0641-x.

Thomas, S., 2008. "Enhanced oil recovery – an overview". *Oil & Gas Science and Technology*, Vol. 63, n. 1, p. 9-19. DOI: 10.2516/ogst:2007060.

Vieira, P. R. M. and Paciornik, S., 2001. "Uncertainty evaluation of metallographic measurements by image analysis and thermodynamic modeling". *Materials Characterization*. Vol. 47, n. 3-4, p. 219-226. DOI: 10.1016/S1044-5803(01)00171-1.

Walmann, T., 1992. "Visualization of transport phenomena in three-dimensional porous media". *Master's Thesis*. University of Oslo.

Yeganeh, M. *et al*., 2016. "Capillary desaturation curve fundamentals". *SPE Improved Oil Recovery Conference*. 11-13 April, Oklahoma, USA. DOI: 10.2118/179574-MS.

7. RESPONSIBILITY NOTICE

The authors are the only responsible for the printed material included in this paper.